Journal of Alloys and Compounds 482 (2009) 308–312

Journal of Alloys and Compounds

journal homepage: www.elsevier.com/locate/jallcom

Raman and infrared study of 100 MeV swift Ag^{8+} heavy ion irradiation effects in $CaSO_4{\cdot}2H_2O$ single crystals

H. Nagabhushana [a,*], B.M. Nagabhushana [b], H.B. Premkumar [c], B.N. Lakshminarasappa [d], Fouran Singh [e], R.P.S. Chakradhar [f]

[a] Department of PG Studies in Physics, Government Science College, Tumkur 572103, India
[b] Department of Chemistry, M.S. Ramaiah Institute of Technology, Bangalore 560054, India
[c] Sri Bhagawan Mahaveer Jain College, J.C. Road, Bangalore 560027, India
[d] Department of Physics, Bangalore University, Bangalore 560056, India
[e] Inter University Accelerator Centre, Aruna Asaf Alimarg, New Delhi 110067, India
[f] Glass Technology Laboratory, Central Glass and Ceramic Research Institute, Council of Scientific & Industrial Research (CSIR), Kolkata 700032, India

ARTICLE INFO

Article history:
Available online 10 April 2009

PACS:
87.64.je
33.20.Ea
33.20.Fb.
36.20.Ng

Keywords:
Quasi crystals
Electron phonon interactions
Atom
Molecule
Ion impact

ABSTRACT

The modifications of calcium sulphate ($CaSO_4{\cdot}2H_2O$) single crystals are investigated by means of Raman and Fourier transform infrared spectroscopy (FT-IR) using 100 MeV Ag^{8+} ions in the fluence range 1×10^{11} to 5×10^{13} ions/cm^2. It is observed that the intensities of the Raman modes decrease with increase in ion fluence. We determined damage cross-section (σ) for all the Raman active modes and found to be different for different Raman modes. Further, FT-IR studies have been carried out to confirm surface amorphisation for a fluence of 1×10^{13} ions/cm^2. It is observed that the absorption peaks at 1132–1156 cm^{-1} corresponds to $\nu_3(SO_4^{2-})$ mode. The decrease in Raman peaks intensity with ion fluence is attributed to degradation of $\nu_3(SO_4^{2-})$ modes present on the surface of the sample.

1. Introduction

Swift heavy ion (SHI) irradiation is a very effective tool for the modification of materials. The energy of the ion is transferred to the solid almost instantaneously in the highly localized volume even in nano meter dimension. Hence, single energetic swift heavy ions can be used to generate non-equilibrium phases with structural and physical properties [1–3]. Though SHI irradiation is complicated and expensive, it is a unique tool to modify the materials by any other process. The important advantage is the flexibility in process parameters such as the energy and type of ion and fluence available for achieving various properties of the resultant material [4].

A swift heavy ion while passing through matter loses its energy either by elastic collisions with nucleus (nuclear stopping power $S_n\{(dE/dx)_n\}$) or by inelastic collisions with electrons (electronic stopping power $S_e\{(dE/dx)_e\}$). In the energy region around 1 MeV/amu the nuclear energy loss becomes negligible and electronic energy loss dominates. It has already been proved that amorphised latent tracks are produced above a threshold value of S_e i.e. S_{eth} ($S_e > S_{eth}$) corresponding to a large electronic excitation. It is well established that irradiation of solids with energetic particles leads to creation of a wide variety of defect states therein. At medium ion energies (keV range), the damage mechanism is due to the nuclear energy loss, whereas at higher energies (MeV–GeV range) it is caused by the electronic energy loss [5–7]. Electronic energy loss plays a dominant role on the whole ion path except in the nuclear stopping region at the end of the ion range. Hence the swift heavy ion effects in matter are essentially related to the strong electronic excitation effects [8]. Therefore, various kinds of materials using different ion irradiation with variable energies to modify the materials are of immense interest in recent times.

Brunetto et al. [9] have studied the amorphisation of diamond by Raman studies using H^+, He^+, Ar^{2+}, Ar^+ with energies 200–400 keV in the fluence range 0.17–4.2 $\times 10^{16}$ ions/cm^2. In all the ions the first order diamond Raman bands area decreases progressively to zero as the ion fluence increases. Amorphous carbon (SP^2 hybridization) is formed during He^+ and Ar^{2+} ion irradiation, while it is not formed with H^+ ions, because the displacement/cm^3 for the highest

* Corresponding author. Tel.: +91 080 23146895; fax: +91 0816 2260220.
E-mail address: bhushanvl@redimail.com (H. Nagabhushana).

0925-8388/$ – see front matter © 2009 Elsevier B.V. All rights reserved.
doi:10.1016/j.jallcom.2009.04.010

H^+ dose are below the amorphisation threshold. The peak position 1545 cm^{-1} shifting towards 1515 cm^{-1} at higher doses. This shift is an indicative of an evolution towards a highly disordered material. Suresh Kumar et al. [10] have studied GaN using 100 MeV Au^{7+} ion irradiation by varying the fluences 1×10^{12} to 5×10^{13} ions/cm^2 at room temperature. The structural studies were investigated using XRD and Raman scattering measurements. XRD results reveal that the intensity of sharp peak of Wurtzite GaN (at $2\theta = 34.5^\circ$) decreases gradually with increase of incident ion fluence. Further, the full width at half maximum (FWHM) increases from 0.087° to 0.27° due to structural damage. The Raman modes (ν_2) shift to lower wavenumber side indicating a compressive strain. Further, increasing the ion fluence, results in disappearance of the ν_2 modes. The Raman peaks were broadened and intensity reduced drastically. This is due to amorphisation of GaN.

Veeramani et al. [11] have studied the CdTe single crystals by SHI irradiation of Ag^{7+} ions with 100MeV energy and fluence in the range 10^{11} to 10^{14} ions/cm^2 and structural damage was investigated by using AFM, XRD and PL. The XRD pattern indicates the prominent peak (1 1 1) show increase of FWHM and reduction in intensity as a function of ion fluence. This indicates that SHIs penetrate the crystal along the trajectory of the ion beam and lead to material modification and distort their lattice. In this process it generates defects and partial amorphisation resulting in a non-crystalline nature. Further the intensity variation is attributed to creation of defects like surface tracks. These surface tracks are created from ion-induced melt due to mechanical stress arising from the thermal expansion. Further PL intensity is reduced after irradiation, which confirms that lattice disorder begins on the surface of the sample due to the high-energy irradiation. This result suggests that the defects created by Ag^{7+} ions on CdTe samples can act either as traps or as non-radiative recombination centers.

Calcium sulphate also known as gypsum is one of the important mineral being used as single drug for specific diseases in Unani system of medicine [12]. Calcium sulphate doped with rare earth elements is an important candidate for personal thermoluminescence dosimeters due to its sensitivity and good thermal stability [13]. The unit cell parameters were found to be $a = 5.68$ Å, $b = 15.18$ Å, $c = 6.51$ Å and $\beta = 118.4^\circ$ with $Z = 4$. The space group is $12/a$ (C_{2h}^6). It has transition sequence of gypsum–bassanite–anhydrite. Previous workers from IR and Raman studies [14,15] have demonstrated that sulphate internal modes were sensitive to the phase changes from temperature and pressure and could effectively be used to probe the structure transitions. However nobody has studied the effect of swift heavy ion irradiation effects on calcium sulphate single crystals. In the present work, an attempt has been made to study 100 MeV Ag^{8+} ion irradiation effects on SO_4^{2-} modes in the $CaSO_4 \cdot 2H_2O$ single crystals with ion fluence.

2. Experimental

In this experiment, transparent $CaSO_4 \cdot 2H_2O$ single crystals cleaved from big block procured at Drug standardization research institute, Madras of thickness ~1 mm × 1 mm × 2 mm was used. The samples were irradiated with 100 MeV Ag^{8+} ions by using a 15 UD Pelletron Accelerator at the Nuclear Science Centre, New Delhi, India [16]. These studies were performed at room temperature in an experimental chamber under vacuum better than 10^{-7} Torr. The beam was scanned over a 1 cm × 1 cm area on the sample using a magnetic beam scanner. The dose of charge accumulated in the sample was measured separately in terms of fluences and the following fluences in the range 1×10^{11} to 5×10^{13} ions/cm^2 were used. The ion currents used were lower than 2 pnA to avoid macroscopic heating of the sample.

Raman spectroscopic studies are performed on the pristine and ion irradiated $CaSO_4 \cdot 2H_2O$ single crystals using a Renishaw In-via Raman spectrometer with 785 nm He–Cd laser and a Leica DMLM optical microscope equipped with 50× objective lens is used to determine the analyzed part of the sample. The laser beam was focused on to the sample using a 50× objective, thus providing a laser spot about 2 μm in diameter. In order to avoid sample degradation during the measurements very low powers were employed (<0.5 mW) and the sample was slowly scanned under the laser beam. Sample degradation due to laser damage could be identified by the observation of a rise in the background in the Raman spectrum as data were being collected. If this was seen to occur, the measurement was rejected and the run was repeated. The system also includes a monochromator, a filter system and CCD. The Raman spectra were taken on the irradiated $CaSO_4 \cdot 2H_2O$ crystals in the range 100–1300 cm^{-1}. Three accumulations for each position with an accumulation time of 10 sec are maintained for all the measurements. The spectra are calibrated using 520 cm^{-1} line of silicon wafer. The data acquisition and analysis are carried out using *WIRE 2.0* software. Fourier transform infrared spectroscopy (FT-IR) measurements were performed in transmission mode on the same set of samples (pristine and ion irradiated $CaSO_4 \cdot 2H_2O$ single crystals). The FT-IR measurements were performed using Bruker instrument from 400 to 1300 cm^{-1}.

3. Results and discussion

Raman spectra of un-irradiated (pristine) and irradiated $CaSO_4 \cdot 2H_2O$ single crystals with 100 MeV Ag^{8+} ions in the fluence range 1×10^{11} to 5×10^{13} ions/cm^2 after appropriate calibration and baseline fitting of the raw data are shown in Fig. 1. The Raman active modes at 411, 484, 610, 1008 and 1137 cm^{-1} are recorded in both pristine and ion irradiated samples. These modes are assigned to ν_2(411, 484 cm^{-1}), ν_4(610 cm^{-1}), ν_1(1008 cm^{-1}) and ν_3(1137 cm^{-1}) SO_4^{2-} modes, respectively. These modes are in good agreement with those reported in the literature [17]. Figs. 2 and 3 show the variation of Raman (1008 cm^{-1}) peak intensity and FWHM as a function of ion fluence. It is observed that the Raman modes intensity decreases, where as the FWHM increases exponentially with ion fluence. The decrease in intensity is faster for 1008 cm^{-1} mode when compared to 411, 484, 610 and 1137 cm^{-1} modes. The mode assignment, peak intensity and FWHM for various Raman active modes are given in Table 1. It is observed that the peak position of intense Raman mode (1008 cm^{-1}) shifted towards lower wavenumber side. Further, it is observed that peak intensity and FWHM decrease with increase of ion fluence. This might be attributed to amorphisation of the sample.

The cross-section (σ) for the destruction of the $CaSO_4 \cdot 2H_2O$ can be observed from the decrease in the Raman peak intensity as a

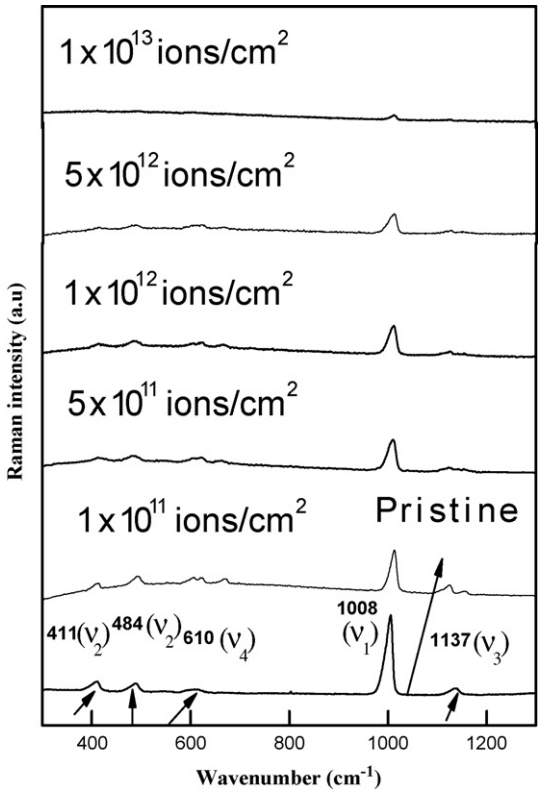

Fig. 1. Raman spectra of pristine and 100 MeV Ag^{8+} ion irradiated $CaSO_4 \cdot 2H_2O$ single crystals.

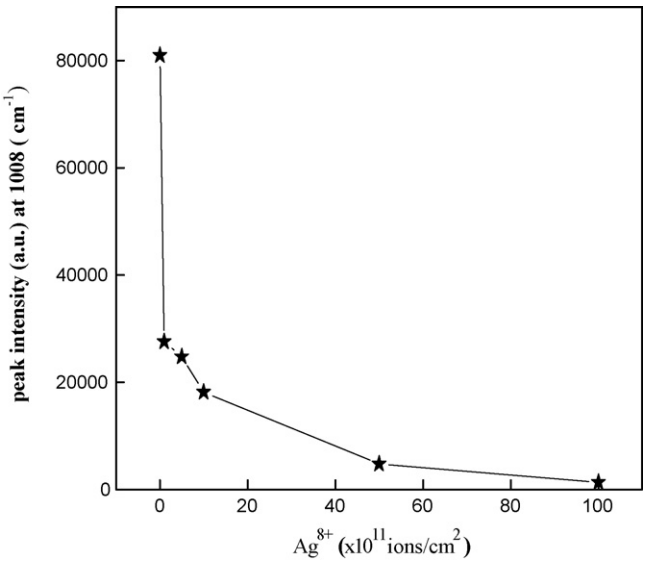

Fig. 2. Variation of Raman peak intensity at 1008 cm^{-1} as a function of Ag^{8+} ion fluence.

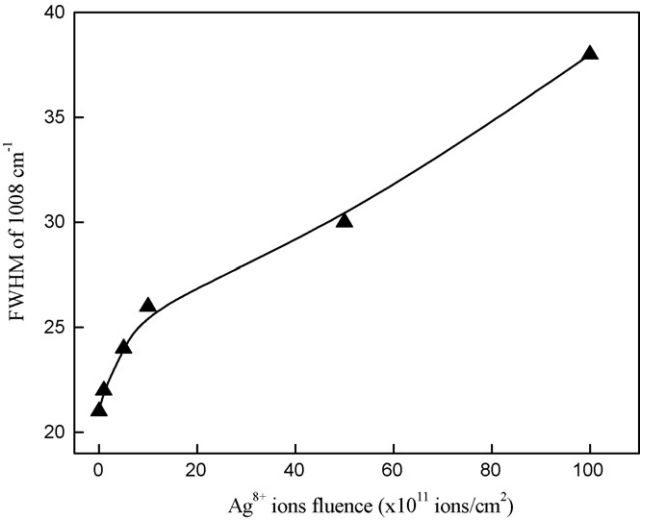

Fig. 3. Variation of FWHM of 1008 cm^{-1} peak as a function of Ag^{8+} ion fluence.

function of ion dose as shown in Fig. 4. Following the analysis suggested in [18] we assume that the areal density N of the $CaSO_4{\cdot}2H_2O$ molecule remaining after irradiation with an ion dose D is given by

$$N = N_0 \exp(-\sigma D)$$

where σ is the cross-section. For the Raman measurements, N is proportional to the integrated Raman intensity. Hence, for the Raman measurements a plot of $\log_{10}[I(D)/I_0]$ versus dose where $I(D)$ is the intensity of a particular Raman peak after a dose D and I_0 is the intensity of the corresponding peak in the unirradiated sample,

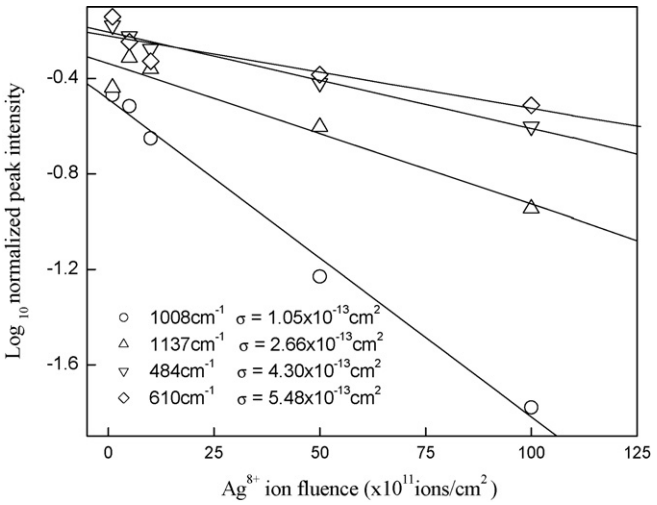

Fig. 4. The diminution of the intensity of the Raman active mode (1008 cm^{-1}) as a function of 100 MeV Ag^{8+} ion fluence displayed as $\log_{10}[I(\Phi)/I_0]$ versus fluence.

should yield a straight line whose slope is the cross-section, σ for the destruction of $CaSO_4{\cdot}2H_2O$ by the ion beam. In Fig. 4, the intensity of the different Raman bands after a given dose $I(D)$, normalized to the intensity of this peak for unirradiated sample Io is plotted as $\log_{10}[I(D)/I_0]$ versus ion fluence. The Raman data when plotted in this way do indeed follow a straight-line dependence. The linear fits to Raman data in Fig. 4 yield a damage cross-section (σ) of different Raman modes. The errors have been estimated on the basis of lines of worst fit taking in to account the uncertainties in each of the data points. It is noticed that all the fundamental Raman active modes having different damage cross-sections/different sensitiveness for ion irradiation. The 1008 cm^{-1} mode has highest cross-section i.e. the most sensitive to get damaged by ion beam. On the other hand the 610 cm^{-1} mode had lowest damage cross-section, is the least affected vibrational mode.

FT-IR studies have been carried out to confirm the surface amorphisation. Fig. 5 shows the FT-IR spectra of pristine and 100 MeV Ag^{8+} ion irradiated $CaSO_4{\cdot}2H_2O$ for a fluence of 1×10^{13} ions/cm^2. The spectrum reveals the characteristic absorption bands of SO_4^{2-} before ion irradiation of the sample. Anbalagan et al. [19] have studied the Indian origin gypsum by FT-IR and Raman spectroscopy. They recorded a strong doublet at 600 and 669 cm^{-1} due to $\nu_4(SO_4^{2-})$ bending vibrations and weak shouldered band at 1000 cm^{-1} is due to $\nu_1(SO_4^{2-})$. The intense bands at 1115 and 1143 cm^{-1} are due to $\nu_3(SO_4^{2-})$, the bands at 420–450 cm^{-1} are attributed to $\nu_2(SO_4^{2-})$ bending vibration. In Raman studies, all the observed vibrational bands of gypsum in the present work were compared with those reported in the literature [20–22]. Prasad et al. [23] have studied the dehydration of natural gypsum single crystals in the temperature range 300–430 K by FT-IR spectroscopy. The fundamental modes of gypsum at 602–669 cm^{-1} are due to $\nu_4(SO_4^{2-})$, the mode at 1005 cm^{-1} is due to $\nu_1(SO_4^{2-})$, the modes at 1117–1167 cm^{-1} are due to $\nu_3(SO_4^{2-})$. The modes at 3405–3495 cm^{-1} due to $\nu_1(H_2O)$ and 3547 cm^{-1} is due to $\nu_3(H_2O)$.

Table 1
Raman bands assignment and peak intensity, FWHM of 1008 cm^{-1} mode in Ag^{8+} ion bombarded calcium sulphate single crystals.

S. no.	Observed Raman bands (cm^{-1})	Band assignments of (SO_4^{2-})	Ion fluence (ions/cm^2)	Peak intensity (a.u.) at 1008 cm^{-1}	FWHM
1	1008	ν_1	1×10^{11}	27557	22
2	411, 484	ν_2	5×0^{11}	24745	24
3	1137	ν_3	1×10^{12}	18183	26
4	610	ν_4	5×10^{12}	4747	30
5			1×10^{13}	1351	38
6			Pristine	80990	21

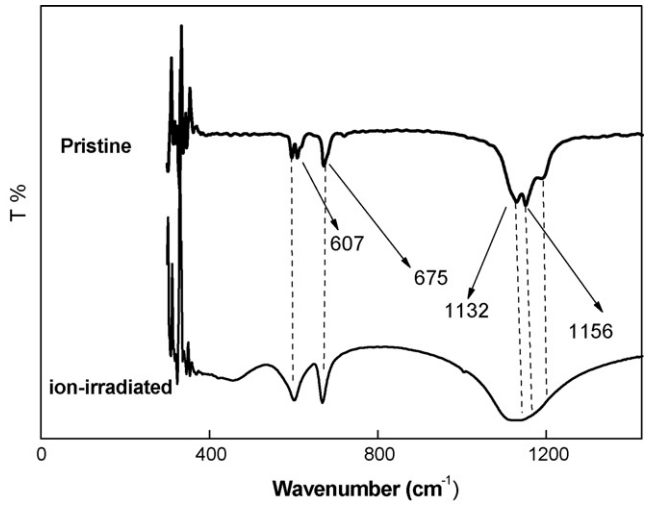

Fig. 5. FT-IR spectra of pristine and 100 MeV Ag^{8+} ion irradiated $CaSO_4{\cdot}2H_2O$ single crystals.

Kloprogge et al. [24] have studied the thermal decomposition of syngenite (K_2 Ca $(SO_4)_2{\cdot}H_2O$) by TGA-DTA, XRD and FT-IR spectroscopy. In IR spectra, The bands at 981 and 1000 cm^{-1} are due to $\nu_1(SO_4{}^{2-})$, the band at 439 cm^{-1} is due to $\nu_2(SO_4{}^{2-})$, the bands at 1110, 1125, 1136, 1148 and 1193 cm^{-1} are due to $\nu_3(SO_4{}^{2-})$, the bands at 604, 617, 644 and 657 cm^{-1} are due to $\nu_4(SO_4{}^{2-})$. In addition to these, –OH liberation mode at 704 cm^{-1}, –OH bending mode at 1631 cm^{-1}, –OH stretching mode at 3248 (symmetric) and 3377 cm^{-1} (anti-symmetric).

It is observed from the figure that in irradiated sample the $\nu_3(SO_4{}^{2-})$ modes at 1132–1156 cm^{-1} completely destructed and the destruction of these modes with irradiation may further enhance the amorphous in nature of the sample. From transport of ions in matter (TRIM) [25] calculations, when the energy of the incident ions is of few keV then nuclear energy loss (S_n) are significant as compared to electronic energy loss (S_e). In the present studies, we have used 100 MeV energy for irradiation and the electronic excitation effect is dominant over the nuclear energy transfer interactions in the near surface region.

Mohanty et al. [26] have studied swift heavy ion irradiated α-Al_2O_3 single crystals irradiated with 190 MeV Ag ions with fluences in the range 10^{11} to 10^{13} ions/cm^2. The pristine and ion irradiated samples were characterized by XRD, PL, FT-IR. The XRD results showed that the intensity of the peaks decreases with increase of ion fluence. This might be due to occurrence of amorphisation. Amorphisation of crystalline surface leads to surface tracks. Surface tracks can be related to the generated beneath the surface. The surface tracks are created from the ion-induced melt due to the mechanical stress arising from the thermal expansion. Further they have studied FT-IR measurements to confirm whether surface amorphisation or bulk amorphisation. The peak at 1400 cm^{-1} corresponds to –OH stretch bond. There is no change in peak positions of Al–OH with fluence. At higher fluence, amorphisation occur without disturbing any –OH bonds. Thus, SHI irradiation leads to surface amorphisation.

As strong electronic excitation dominates the damage process of irradiation, the $SO_4{}^{2-}$ modes may highly excited due to electron–electron and electron–phonon interaction as a result the local temperature of the lattice is raising abruptly and the thermal motion of the atoms is increased. The disordered atoms will contribute to the internal stress and thus the Raman and IR peaks are broader in ion-irradiated samples [27]. The decrease in Raman intensity might be attributed to the destruction of the surface chemical species [$\nu_3(SO_4{}^{2-})$] because of the energy deposited through S_e during SHI irradiation and formation of non-radiative recombination centers at higher fluences. The irradiation effects may lead to the restructuring of the chemical species because of the energy deposited through electronic energy loss during the process of SHI irradiation and formation of ion induced defects leading to non-radiative recombination centers. These two processes are simultaneous consequences of irradiation and they compete with each other [28]. The degradation/enhancement in Raman peaks intensity might be due to balance between these two effects. The FWHM and broadening and sharp reduction in intensity of the Raman modes indicates that SHI penetrates the crystal along the trajectory of the ion beam and lead to material modification. In this process the point defects are generated in the lattice due to atomic displacements caused by ions, neutrons and fast electrons. However, the irradiation fluence must be very high to form complex defects from random association of point defects. Since SHI irradiation is a high-density excitation they generate a very high defect density along the ion track [29]. The intensity variation can be attributed to the creation of defects like surface tracks. The surface tracks are created from the ion-induced melt due to mechanical stress [30,31]. Atomic force microscopy (AFM) and glancing angle X-ray diffraction (GXRD) is an effective tool for examining surface modifications/partial/complete amorphisation of the sample.

4. Conclusion

The Raman and Infrared studies of 100 MeV Ag^{8+} ion irradiated $CaSO_4{\cdot}2H_2O$ single crystals have been studied in the fluence range 1×10^{11} to 5×10^{13} ions/cm^2. The Raman peaks intensity decreases with increase of Ag^{8+} ion fluence. This decrease in peaks intensity is attributed to destruction/amorphisation of $\nu_3(SO_4{}^{2-})$ mode present on the surface of the sample. The sensitivity of damage for all Raman active modes is different under ion irradiation.

Acknowledgments

The authors wish to express their sincere thanks to Dr. D.K. Avasthi, Nuclear Science center (NSC), New Delhi, for useful discussion, besides his constant help and encouragement in this work. H.N. thanks to NSC for the award of Fellowship under UFUP scheme. Dr. RPSC thanks Dr. H. S Maiti, Director, CGCRI and Dr. Ranjan Sen, Head, GTL lab, CGCRI for their constant support and encouragement.

References

[1] D.K. Avasthi, Vacuum 47 (1996) 1249.
[2] W. Bolse, Nucl. Instrum. Methods B 244 (2006) 8.
[3] M. Toulemonde, C. Trautmann, E. Balanzat, K. Hjort, A. Weidinger, Nucl. Instrum. Methods B 216 (2004) 1.
[4] P.S. Chaudhari, T.M. Bhave, Renu Pasricha, Fouran Singh, D. Kanjilal, S.V. Bhoraskar, Nucl. Instrum. Methods B 239 (2005) 185.
[5] J. Liu, M.D. Hou, C. Trautmann, R. Neumann, C. Muller, Z.G. Wang, Q.X. Zhang, Y.M. Sun, Y.F. Jin, H.W. Liu, H.J. Gao, Nucl. Instrum. Methods B 212 (2003) 303.
[6] J. Winter, H. Kuzmany, Phys. Rev. B 88 (2000) 51.
[7] C.E. Foerster, F.C. Serbena, C.M. Lepienski, D.L. Baptista, F.C. Zawislak, Nucl. Instrum. Methods B 148 (1999) 634.
[8] E. Balanzat, N. Betz, S. Bouffard, Nucl. Instrum. Methods. B 105 (1995) 46.
[9] R. Brunetto, G.A. Baratta, G. Strazzulla, J. Phys: Conf. Ser. 6 (2005) 120.
[10] V. Suresh Kumar, M. Senthil Kumar, P. Puviarasu, J. Kumar, T. Mohanty, D. Kanjilal, K. Asokan, A. Tripathi, M. Fontana, A. Camarani, Semicond. Sci. Technol. 22 (2007) 511.
[11] P. Veeramani, M. Haris, D. Kanjilal, K. Asokan, S. Moorthy Babu, J. Phys. D: Appl. Phys. 39 (2006) 2707.
[12] National formulary of Unani, medicine part-I, 1st Edn., Government of India, Ministry of Health and Family Welfare (Department of Health), New Delhi, India.
[13] M. Maghrabi, T. Karali, P.D. Townsend, A.R. Lakshmanan, J. Phys. D: Appl. Phys. 33 (2000) 477.
[14] P.S.R. Prasad, A. Pradhan, T.N. Gowd, Curr. Sci. 10 (2001) 1203.
[15] P.S.R. Prasad, N. Ravikumar, A.S.R. Krishnamurthy, L.P. Sharma, Curr. Sci. 75 (1998) 1410.
[16] G.K. Mehta, A.P. Patro, Nucl. Instrum. Methods A 268 (1998) 334.

[17] P.S.R. Prasad, J. Raman Spectrosc. 30 (1999) 693.
[18] S. Prawer, K.W. Nugent, S. Biggs, D.G. McCulloch, W.H. Leong, A. Hoffman, R. Kalish, Phys. Rev. B 52 (1995) 841.
[19] G. Anbalagan, S. Mukundakumari, K. Sakthi Murugesan, Vib. Spectrosc. (2009), doi:10.1016/j.vibspec.2008.12.004.
[20] C.D. Cooper, J.F. Mustard, ICARUS 158 (2002) 42.
[21] N. Krishnamurthy, V. Scoots, Can. J. Phys. 49 (1971) 885.
[22] L.P. Sharma, P.S.R. Prasad, N. Ravikumar, J. Raman. Spectrosc. 29 (1998) 851.
[23] P.S.R. Prasad, V. Krishna Chaitanya, K. Shiva Prasad, D. Narayana Rao, Am. Minerol. 90 (2005) 672.
[24] J.T. Kloprogge, Zhe Ding, W.N. Martens, R.D. Schuiling, L.V. Duong, R.L. Frost, Thermochim. Acta 417 (2004) 143.
[25] J.F. Ziegler, J.P. Biersack, U. Littmark, The Stopping and Range of Ions in Solids, Pergamon, Oxford, U.K, 1985.
[26] T. Mohanty, N.C. Mishra, F. Singh, U. Tiwari, D. Kanjilal, Nucl. Instrum. Methods B 212 (2003) 179.
[27] Y.F. Jin, H.X. Tian, E.Q. Xie, J. Liu, Z.G. Wang, Y. Sun, Z.Y. Zhu, Nucl. Instrum. Methods B 193 (2002) 288.
[28] T.M. Bhave, S.S. Hullavarad, S.V. Bhoraskar, S.G. Hegde, D. Kanjilal, Nucl. Instrum. Methods B 156 (1999) 121.
[29] A. Alghamdi, P.D. Townsend, Nucl. Instrum. Methods. B 46 (1990) 133.
[30] G. Szenes, Nucl. Instrum. Methods B 191 (2002) 27.
[31] T. Nakazawa, A. Naito, T. Aruga, V. Grismanovs, Y. Chimi, A. Iwase, S. Jitsukawa, J. Nucl. Mater. 367 (2007) 1398.